The 9th European Congress on Computational Methods in Applied Sciences and Engineering
ECCOMAS Congress 2024
3–7 June 2024, Lisboa, Portugal

LOW MACH PRECONDITIONING FOR HARMONIC BALANCE SOLVERS

PIERRE SIVEL[1] AND CHRISTIAN FREY[2]

German Aerospace Center (DLR), Linder Höhe, 51147 Cologne, Germany

[1] pierre.sivel@dlr.de, [2] christian.frey@dlr.de

Key words: Computational Fluid Dynamics, Low Mach Preconditioning, Harmonic Balance

Summary. Density-based solvers suffer from a decrease in solution quality and convergence rate as the Mach number decreases. Previous studies have demonstrated that low Mach preconditioning improves the performance of density-based steady-state solvers at low Mach numbers. Applying a similar procedure, this study presents a low Mach preconditioning approach for harmonic balance solvers, which enhances the solution quality and optimizes convergence rates of frequency-domain computations in the low Mach regime.

The convergence rate is improved by multiplying the time derivative with a preconditioning matrix, equalizing the acoustic and convective propagation velocities. However, for unsteady computations, the preconditioner introduces a frequency dependence to the acoustic propagation velocity. Thus, frequency-dependent preconditionining parameters are required for harmonic balance computations.

Excessive numerical dissipation in the Roe solver causes inaccuracies at low Mach numbers. To address this, a preconditioned Roe solver for unsteady computations is employed, ensuring correct Mach number scaling in the artificial diffusion.

The preconditioned harmonic balance solver is applied to a low Mach cylinder and the results are compared with non-preconditioned computations and experimental data. This comparison highlights shortcomings of the non-preconditioned Roe scheme in predicting unsteady flows and demonstrates that preconditioned computations are in excellent agreement with the experiments across all Mach numbers. Furthermore, the use of a frequency-dependent preconditioner is shown to achieve the fastest convergence.

1 INTRODUCTION

Harmonic balance (HB) solvers have gained popularity in CFD for the efficient computation of time-periodic flows [1]. The solution is expressed in terms of truncated Fourier series about a base frequency, which yields a system of equations for the harmonics of the solution. This system is solved in the frequency-domain using efficient steady-state solution algorithms, significantly reducing computational cost compared to time-domain methods [2].

A drawback of HB solvers is that a priori knowledge of the solution's base-frequency is required. When the frequency itself depends on the solution, e.g., the vortex shedding frequency of a cylinder, this requirement may not be fulfilled. A discrepancy between the solution's frequency and the solver frequency can lead to severe convergence issues. Therefore, HB solvers have

recently been extended with frequency adaptation algorithms, which correct the solver frequency at runtime [3].

To converge reliably, these algorithms require an accurate prediction of the solution. It is well known that density-based solvers are stiff and inaccurate when applied to low Mach flows [4, 5, 6]. The solver's performance can be enhanced using low Mach preconditioning, which is split in two categories. Iterative preconditioning accelerates the convergence by multiplying the time derivative of the governing equations with a preconditioning matrix. This equalizes the acoustic and convective propagation velocities, elevating the stiffness arising from the large discrepancy between these velocities [6]. Preconditioning of the artificial dissipation reduces the artificial dissipation introduced by the Roe scheme at low Mach numbers, thereby greatly improving the accuracy. To that end, the Roe matrix is rewritten based on preconditioned convective fluxes [4].

Low Mach preconditioning has been successfully applied to steady-state computations [7, 8]. However, in HB computations, steady preconditioning methods can reduce the convergence rate and accuracy of the solution rather than improving them. Only a few publications have explored low Mach preconditioning for HB solvers [9, 10, 11], and none consider HB equations solved in the frequency-domain. Therefore, this paper proposes, for the first time, a preconditioning method for the HB solver in the frequency domain.

The HB method is briefly outlined, followed by the proposal of a novel HB preconditioner that combines an adaptation of the preconditioned Roe scheme (PRoe) for unsteady flows [12] with a frequency-dependent iterative preconditioner. This HB preconditioner is then applied to a laminar cylinder with vortex shedding at low Mach numbers and validated against experimental data. The results are compared with both non-preconditioned computations and computations using the steady preconditioner.

2 HARMONIC BALANCE

The HB equations are derived from the unsteady time-domain governing equations:

$$\frac{\partial q}{\partial t} + R(q) = 0, \tag{1}$$

where q is the state vector, t is the physical time, and R is the nonlinear residual containing all fluxes and source terms. Assuming temporal periodicity, the solution is approximated as a truncated Fourier series about a base frequency ω:

$$q\left(t, x, y, z\right) = \mathrm{Re}\left(\sum_{k=0}^{K} \widehat{q}_k\left(x, y, z\right) e^{ik\omega t}\right). \tag{2}$$

Here, $\widehat{q}_k$ represents the Fourier coefficient of the k-th harmonic, while K denotes the number of harmonics employed to approximate the solution. The substitution of the Fourier series (2) into the governing equation (1) yields the HB equations:

$$ik\omega\widehat{q}_k + \widehat{R}_k(q) = 0, \quad \text{for} \quad k = 0, \ldots, K. \tag{3}$$

The system is solved using a mixed frequency-domain and time-domain approach, whereby equations (3) are solved in the frequency-domain, but the harmonics of the nonlinear residual $\widehat{R}_k$ are computed in the time domain. To this end, the time-domain solution q is reconstructed

at equidistant sampling points over one period. The nonlinear residual R is computed at each sampling point and its harmonics $\widehat{R}_k$ are obtained using a discrete Fourier transform. The solution procedure and the discretization of the HB system are described in detail in [2].

3 LOW MACH PRECONDITIONING

3.1 Iterative Preconditioning

The main objective of iterative preconditioning is to improve the convergence of low Mach simulations by artificially reducing the acoustic velocity to the same magnitude as the convective velocity. This is accomplished by multiplying the pseudo-time derivative of the governing equations with the preconditioning matrix P^{-1} [13]

$$P^{-1}\frac{\partial \widehat{q}_k}{\partial \tau} + ik\omega\widehat{q}_k + \widehat{R}_k(q) = 0, \quad \text{for} \quad k = 0, \dots, K \tag{4}$$

where τ is the pseudo-time. In this paper, the preconditioning matrix proposed by Turkel [6] is employed, which in entropy variables $q_S = (\rho, u, v, w, S)$ is expressed as

$$P_S^{-1} = \operatorname{diag}\left(1/\beta^2, 1, 1, 1, 1\right). \tag{5}$$

Here, ρ denotes the density, u, v, w the cartesian velocity components and S the entropy. The preconditioner is controlled by the preconditioning parameter β^2. For steady-state computations, it is defined as

$$\beta^2_{\text{steady}} = \min\left(1, \max\left(\underbrace{k_\beta \text{Ma}^2}_{\text{(A)}}, \underbrace{\left(\frac{10\mu}{\rho a \Delta h}\right)^2}_{\text{(B)}}, \underbrace{\frac{\Delta p}{\rho a^2}}_{\text{(C)}}, \underbrace{\beta^2_{\min}}_{\text{(D)}}\right)\right), \tag{6}$$

where, Ma is the local Mach number, Δp is the pressure difference between neighboring cells, μ is the molecular viscosity, a is the speed of sound and Δh is a characteristic cell length [8]. The convective and acoustic velocities are equalized by (A), which defines β^2 as a function of Ma^2 [13]. Empirical studies performed by the author have demonstrated that adding a factor of $k_\beta = 10 - 100$, substantially improves the stability while only slightly reducing the convergence rate. In the case of viscous computations with very small Reynolds numbers, (B) equalizes the acoustic speed to the diffusive speed instead of the convective speed [14]. The preconditioned system can potentially amplify strong local pressure fluctuations in the flow [15]. Consequently, (C) increases β^2 in the presence of large local pressure differences between neighboring cells. To prevent the preconditioning matrix from becoming singular for $\text{Ma} \to 0$, a user-defined lower bound (D) is introduced [13]. Finally, the preconditioner is disabled in the supersonic regime by ensuring $\beta^2 \leq 1$. For $\beta^2 = 1$, the preconditioning matrix becomes the identity matrix and the non-preconditioned system is retrieved. For HB simulations, β^2 is calculated based on time-average quantities, which coincide with the zeroth harmonic of the solution.

When preconditioning the HB system as in (4), the preconditioned acoustic propagation velocity is a function of the frequency ω. Accordingly, in order to equalize the propagation velocities, it is necessary to extend (6) in a manner that takes into account this frequency dependence. A frequency-dependent preconditioning parameter is derived based on the work of Venkateswaran and Merkle [5] on iterative preconditioning for unsteady time-domain simulations. Here, an unsteady Mach number was introduced, which controls the preconditioner based on the size

of the physical time step. This unsteady Mach number is rewritten as a function of the solver frequency

$$\mathrm{Ma}_{\mathrm{hb},k} = \frac{L\omega_k}{2\pi^2 a}, \tag{7}$$

where L is a characteristic length of the simulation, typically chosen as the domain size. The definition of the preconditioning parameter is then extended to

$$\beta^2_{\mathrm{HB},k} = \min\left(1, \max\left(\beta^2_{\mathrm{steady}}, \mathrm{Ma}^2_{\mathrm{hb},k}\right)\right). \tag{8}$$

When $\omega \to 0$, the HB system behaves like a steady-state computation and $\beta^2_{\mathrm{HB},k} = \beta^2_{\mathrm{steady}}$. For large frequencies, $\mathrm{Ma}_{\mathrm{hb},k} > 1$disables the preconditioner since the non-preconditioned system is already optimally conditioned.

In order to maximize the convergence rate across all harmonics, the computation of frequency-dependent preconditioning parameter $\beta^2_{\mathrm{HB},k}$ and the application of the preconditioner is performed for each harmonic individually. This approach is therefore called individual preconditioning.

3.2 Preconditioned Dissipation

The artificial dissipation of the Roe scheme [16] between two cells is

$$F_{\mathrm{d,Roe}} = -\frac{1}{2}|\widetilde{D}|\Delta q, \tag{9}$$

where Δq is the difference vector between the left and right face-state and the tilde denotes quantities based on Roe-averaging [16]. The Roe matrix $|\tilde{D}|$ is computed based on the eigenvectors R and the eigenvalues λ_i of the convective flux Jacobian $\tilde{D}$

$$|\widetilde{D}| = R|\Lambda|R^{-1} \quad \text{with} \quad |\Lambda| \;=\; \mathrm{diag}\left(|\lambda_1|, |\lambda_2|, |\lambda_3|, |\lambda_4|, |\lambda_5|\right). \tag{10}$$

At low Mach numbers, the Roe scheme's artificial dissipation scales poorly, leading to an inaccurate prediction of convective flows [17]. A common approach to retrieve proper scaling is to redefine the Roe matrix based on the low Mach preconditioned convective fluxes [18, 19]. This yields the so-called PRoe scheme with the artificial dissipation

$$F_{\mathrm{d,P\text{-}Roe}} = -\frac{1}{2}\widetilde{P}^{-1}|\widetilde{P}\widetilde{D}|\Delta q. \tag{11}$$

However, in unsteady computations, PRoe excessively dampens acoustic waves [9]. To maintain the accuracy of PRoe for convective flows, while simultaneously reducing its dampening effect on acoustic waves, Potsdam et al. [12] proposed an adapted preconditioned Roe scheme for unsteady time-domain simulations

$$F_{\mathrm{d,Potsdam}} = -\frac{1}{2}\widetilde{P}_\mathrm{u}^{-1}\left(|\widetilde{P}_\mathrm{u}\widetilde{D}|L_\mathrm{u} + |\widetilde{P}_\mathrm{s}\widetilde{D}|L_\mathrm{s}\right)\Delta q. \tag{12}$$

In this approach, quantities denoted with the subscripts u are based on the HB preconditioning parameter for the first harmonic $\beta^2_{\mathrm{HB},1}$, while those denoted with the subscript s are based on the steady preconditioning parameter $\beta^2_{\mathrm{steady}}$. The concept of this approach is revealed through the use of temperature variables $q_T = (p, u, v, w, T)$, for which the matrices $L_{\mathrm{u/s}}$ become

$$L_{\mathrm{u},T} = \mathrm{diag}\left(1,0,0,0,0\right) \quad \text{and} \quad L_{\mathrm{s},T} = \mathrm{diag}\left(0,1,1,1,1\right). \tag{13}$$

Here, T is the temperature and p is the pressure. In other words, this approach preserves the improved diffusion of PRoe for the convective temperature and velocity fields, while reducing the dissipation associated with acoustics by adapting the pressure field's dissipation [12].

Despite being derived based on different iterative preconditioning parameters, the definition for β^2 and respectively P, are not required to be the same between the iterative preconditioner and the preconditioned dissipation. The different preconditioning methods can be employed independently of each other [19].

4 LAMINAR CYLINDER

The computations presented in this work are performed with the CFD solver TRACE, developed by the German Aerospace Center (DLR) in close cooperation with MTU Aero Engines. TRACE is a hybrid finite-volume multi-block solver for the compressible RANS and URANS equations, with a particular focus on turbomachinery applications [20]. The low Mach preconditioner is implemented in TRACE's HB solver to compute the flow around a cylinder at low Mach numbers. The farfield Mach number ranges from $\mathrm{Ma}_\infty = 0.1$ to 0.0001. The flow is intentionally maintained in the incompressible regime, in order to obtain a near Mach-independent solution [21]. To allow unsteady vortex shedding behind the cylinder, while maintaining laminar flow, the Reynolds number of the cylinder is varied between $\mathrm{Re} = 75$ and 175. The changes in the Mach number and the Reynolds number are achieved by modifying the farfield velocity and adjusting the molecular viscosity accordingly.

In the first computations, the cylinder's shedding frequency is determined as a function of the Reynolds number, in accordance with the correlations presented by Fey et al. [22]

$$\mathrm{St} = 0.2684 + \frac{-1.0356}{\sqrt{\mathrm{Re}}}, \tag{14}$$

with the relation between the frequency f and the Strouhal number St

$$f = \mathrm{St}\frac{d}{u_\infty}. \tag{15}$$

Here, the subscript ∞ denotes quantities at the farfield boundary and d is the diameter of the cylinder.

The computational domain comprises 329 equidistant cells around the cylinder and 471 cells normal to the cylinder wall with a stretching ratio of 1.01. The first cell size at the cylinder is set to ensure a non-dimensional cell size of $y^+ < 1$ for all Mach numbers and Reynolds numbers. Accordingly, the cylinder wall is modeled as a non-slip wall with low-Reynolds resolution. The outer boundary is placed 200 cylinder diameters away from the center of the computational domain, to avoid any spurious interactions between the cylinder's wake and the domain's boundary. Here, the simplified farfield boundary condition for incompressible flows, as presented by Hejranfar and Kamali-Moghadam [23] is applied. All boundary conditions are applied in the time-domain during the computation of the nonlinear residual at each sampling point.

The convective fluxes are discretized with the Roe scheme [16] and elevated to second-order accuracy using the MUSCL reconstruction [25] with the van Albada limiter [26]. For preconditioned computations, the Roe scheme is replaced by either PRoe or Potsdam's Roe scheme. The viscous fluxes are discretized with a central scheme. In the computed Reynolds

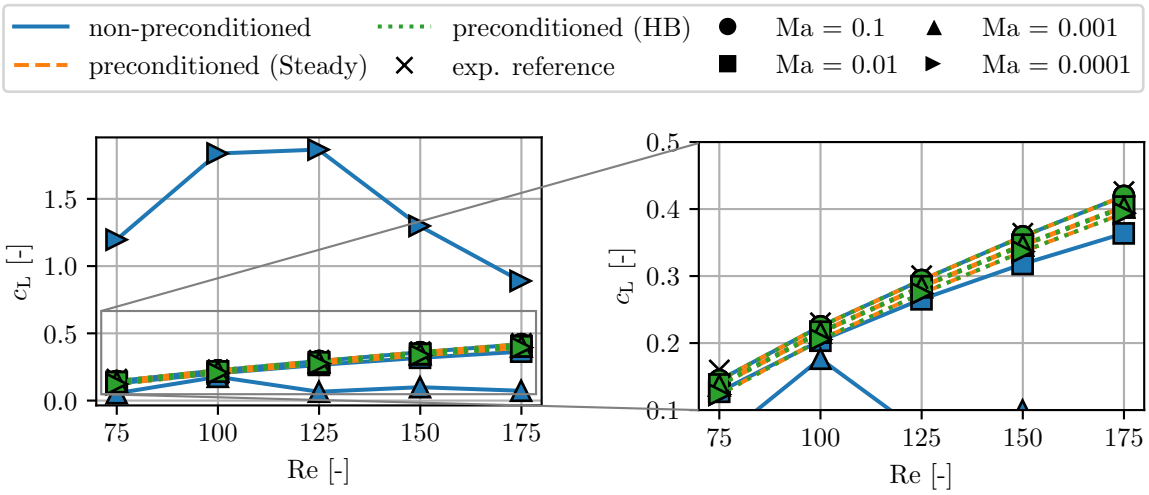

Figure 1: Root-mean-square of the cylinder's lift coefficient c_L over the Reynolds number compared with experimental data presented by Norberg [24].

number range, the cylinder remains laminar. Therefore, no turbulence model or transition model is required. The governing equations are solved with an implicit Euler backwards scheme and local pseudo-time marching [3]. The unsteady flow is resolved with four harmonics and the nonlinear residual is reconstructed at 21 equidistant sampling points per period.

The computations are initialized with a constant solution corresponding to the farfield state. To speed up the development of the unsteady wake of the cylinder, an oscillating mode with an amplitude of 1% of the cylinder's diameter is applied to the cylinder for the first 10 000 iterations.

The following section presents a comparative analysis of three preconditioning configurations for the HB solver:

- **non-preconditioned**: Uses the Roe scheme (9) without iterative preconditioning.
- **preconditioned (steady)**: Uses PRoe (11) with iterative preconditioning based on the steady-state preconditioning parameter β^2_{steady} (6).
- **preconditioned (HB)**: Uses Potsdam's Roe scheme (12) with individual iterative preconditioning based on the HB preconditioning parameters $\beta^2_{\text{HB},k}$ (8).

For all preconditioned computations, the user-defined lower bound for the preconditioning parameter is $\beta_{\min} = 1e{-}10$ and the stabilization constant is $k_\beta = 50$. For the HB preconditioner the characteristic length L is that of the computational domain.

Figure 1 compares the root-mean-square of the cylinder's lift coefficient with experimental results presented in [24]. The lift coefficient is computed according to

$$c_L = \frac{F_L}{\frac{1}{2}\rho_\infty u_\infty dh}. \tag{16}$$

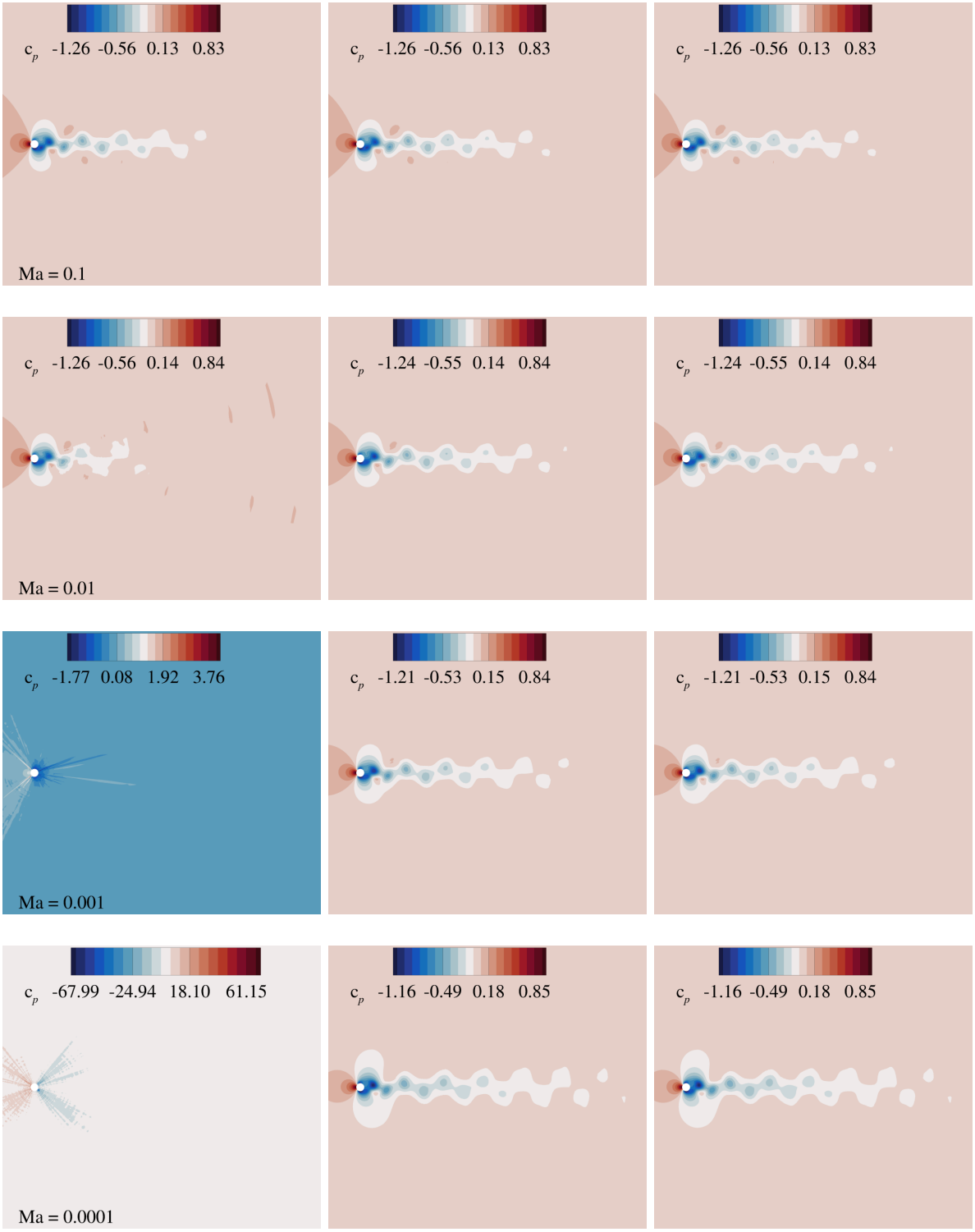

(a) non-preconditioned (b) preconditioned (Steady) (c) preconditioned (HB)

Figure 2: Contours of the pressure coefficient c_p reconstructed at $t = 0$ s and Re $= 125$. The rows contain computations of the same Mach number, while the comlumns contain computations performed with the same preconditioning configurations.

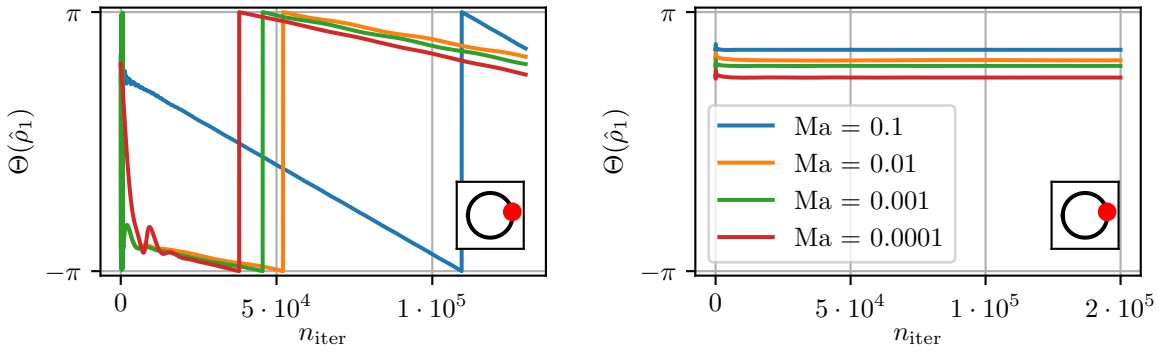

(a) fixed frequency

(b) frequency adaptation

Figure 3: Phase of the density's first harmonic over the pseudo-time iterations at a probe on the cylinder. Thes computations were performed with HB preconditioning at Re = 125. The red dot on the cylinder represents the probe's position.

where, F_{L} is the lift and h is the depth of the cylinder. At Ma = 0.1, the non-preconditioned solution presents a high level of agreement with the experimental reference, accurately reflecting the increase in lift with increasing Reynolds number. At Ma = 0.01, this trend is still maintained, but the lift is underpredicted with an increasing error for higher Reynolds numbers. Below Ma < 0.001, the non-preconditioned solver fails to match the experimental results. In contrast, the preconditioned computations accurately capture the relation between the lift and the Reynolds number for all Mach numbers. A slight decrease in the lift coefficient is observed with decreasing Mach number.

Figure 2 presents a more detailed examination of the flow field at Re = 125, displaying the contours of the pressure coefficient reconstructed from the HB solution at $t = 0\,\text{s}$. The pressure coefficient is calculated following

$$c_p = \frac{p - p_\infty}{\frac{1}{2}\rho_\infty u_\infty^2}. \tag{17}$$

In accordance with the results in Fig. 1, at Ma = 0.1, the solutions are consistent for all preconditioning configurations. At Ma = 0.01, the non-preconditioned computation still develops a vortex street, however, the excessive dissipation of the Roe scheme significantly shortens the wake. For Mach numbers below 0.001, the non-preconditioned solver yields non-physical results, which develop no wake, reach pressures exceeding than the farfield stagnation pressure and exhibit strong numerical artifacts. This lack of physicality in the solution is responsible for the significant errors in the prediction of the cylinder's lift coefficient. In contrast, both preconditioned configurations yield consistent development of a vortex street across all Mach numbers. However, the amplitude of the pressure coefficient decreases slightly with decreasing Mach number, which explains the observed decline in lift. It is noteworthy that PRoe does not introduce any inaccuracies compared to Potsdam's Roe scheme. Both methods yield identical solutions even at the lowest Mach numbers.

In the present computations, the frequency for the HB solver is an empirical estimation of the cylinder's shedding frequency. However, this estimation may differ from the shedding frequency

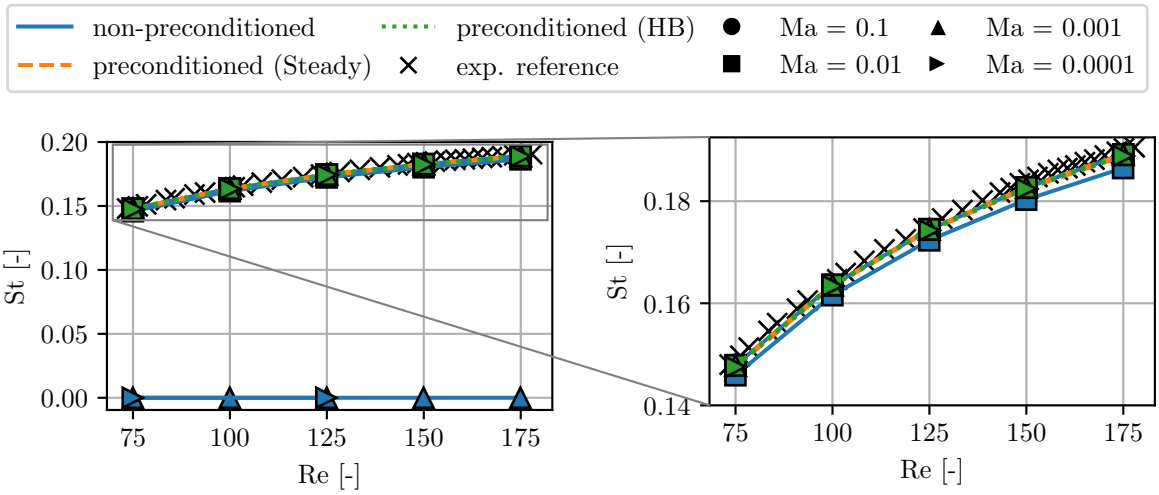

Figure 4: Strouhal numbers predicted by the frequency adaptation algorithm over the Reynolds number compared with the experimental data presented by Williamson [27]

predicted by the solver. This discrepancy manifests itself in the form of a constant shift in the phase of the solution's harmonics. For the computations using the HB preconditioner at $\mathrm{Re} = 125$, Figure 3a, visualizes this phase shift in the first harmonic of the density, indicating a discrepancy between the solver frequency and the shedding frequency.

In order to eliminate the frequency discrepancy and to obtain a converged phase in the higher harmonics, a frequency adaptation algorithm is employed, which corrects the solver frequency at run time. For details on the frequency adaptation algorithm, the reader is referred to [3]. Figure 3b depicts the phase of the density's first harmonic over the pseudo-time iterations using the frequency adaptation algorithm. It demonstrates that correcting the frequency removes the phase shift, indicating that the solver and shedding frequencies are now matching.

The frequencies resulting from the adaptation algorithm are presented in Figure 4 in the form of their respective Strouhal number and are compared with the experimental data presented by Williamson [27]. The preconditioned computations show excellent agreement with the experiments, with a maximum deviation of 0.9 % from the reference. In contrast to the lift coefficient, the predictive quality is maintained across all Mach numbers. At $\mathrm{Ma} = 0.1$, the non-preconditioned computations remain consistent with the preconditioned results. A reduction in the Mach number to $\mathrm{Ma} = 0.01$ already results in a decrease in the frequency, yielding a consistent underestimation of the Strouhal number across all Reynolds numbers by 1.5 % to 2 %. Figure 2 illustrated that no unsteady wake formed in the non-preconditioned computations, as the Mach number is further decreased below $\mathrm{Ma} \leq 0.01$. Consequently, the frequency adaptation algorithm is unable to identify any dominant frequency in the solution and reduces the solver frequency to zero, effectively resulting in a steady-state computation.

Finally, the influence of iterative preconditioning on the convergence of the frequency adaptation is analyzed. The Roe scheme not only leads to inaccurate solutions, but also hinders the convergence of the computation. Therefore, for all three preconditioning configurations, the respective Roe scheme is replaced by Potsdam's Roe scheme. This guarantees an accurate

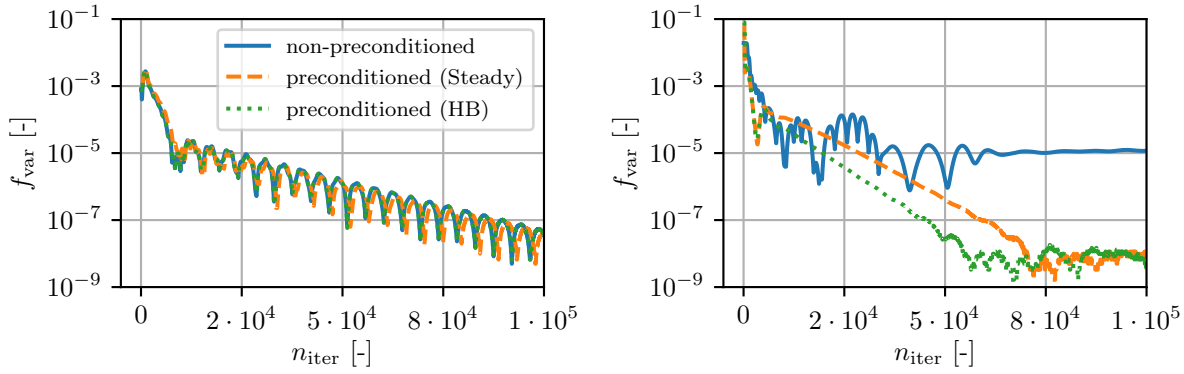

(a) Ma = 0.1

(b) Ma = 0.0001

Figure 5: Relative variation of the frequency over an interval of 1000 iteration using the frequency adaptation algorithm. Potsdam's Roe scheme is applied for all preconditioning setups.

solution and isolates the influence of the different iterative preconditioners. Figure 5 shows the convergence history of the Strouhal number for Re = 125 at Ma = 0.1 and Ma = 0.0001. Here, convergence is evaluated based on the variation of the Strouhal number over an interval of 1000 iterations divided by the mean value over the same interval. This gives a relative accuracy in terms of the final converged frequency of each computation. For Ma = 0.1 the convergence rates are consistent across all three preconditioning setups, reducing relative variations of the frequency to 1e-7 after about 90 000 iterations. For Ma = 0.0001, the convergence rate of the non-preconditioned computation is significantly reduced, still having relative variations of 1e-5 after 400 000 iterations, at which point the simulation ended. In contrast, the steady preconditioner reaches variations of 1e-7 after about 70 000 iterations. The frequency-dependent preconditioner converges even faster, requiring only about 45 000 iterations to reduce the variations to 1e-7, 35% fewer iterations than the steady preconditioner.

5 CONCLUSIONS

This paper presented a novel approach to low Mach preconditioning in the context of HB solvers. The approach combines Potsdam's adaptation of the Roe scheme for unsteady low Mach computations with a frequency-dependent iterative preconditioning approach that optimizes the preconditioning parameters for each harmonic equation individually. The method was applied to HB simulations of a laminar cylinder test case and compared with the steady preconditioned and non-preconditioned computations. The main conclusions drawn from these results are:

- At Ma = 0.1, the preconditioned computations yield consistent solutions to the non-preconditioned solver, demonstrating that preconditioning does not alter the performance of the HB solver at high Mach numbers.
- As Mach numbers decrease, the Roe scheme becomes increasingly inaccurate, leading to unphysical solutions below Ma $\leq$ 0.001.
- At low Mach numbers, the preconditioned Roe schemes significantly improve the solution quality and are necessary to reliably use the HB solver with frequency adaptation algorithms.

Contrary to findings in the literature, PRoe did not yield any inaccuracies for unsteady low Mach computations of the cylinder. Therefore, no further improvement of the solution was achieved by using Potsdam's Roe scheme.

- Preconditioning leads to a significant increase in convergence speed in the low Mach regime compared to the non-preconditioned solver and yields similar convergence rates at both high and low Mach numbers. The novel frequency-dependent preconditioner further accelerates convergence by approximately 35% compared to the steady preconditioner.

REFERENCES

[1] K. C. Hall, J. P. Thomas, and W. S. Clark. Computation of Unsteady Nonlinear Flows in Cascades Using a Harmonic Balance Technique. *AIAA Journal*, 2002.

[2] C. Frey, G. Ashcroft, H.-P. Kersken, and C. Voigt. A Harmonic Balance Technique for Multistage Turbomachinery Applications. In *Proceedings of ASME Turbo Expo 2014*, 2014.

[3] C. Frey, J. Backhaus, and G. Ashcroft. Efficient and Robust Implicit Solvers for Unsteady Flow Problems Using Harmonic Balance. In *Proceedings of 9th European Congress on Computational Methods in Applied Sciences and Engineering*, 2024.

[4] B. van Leer, W.-T. Lee, and P. Roe. *Characteristic Time-Stepping or Local Preconditioning of the Euler Equations*. 1991.

[5] S. Venkateswaran and C. Merkle. Dual time-stepping and preconditioning for unsteady computations. In *33rd Aerospace Sciences Meeting and Exhibit*. jan 1995.

[6] E. Turkel. Preconditioned methods for solving the incompressible and low speed compressible equations. *Journal of Computational Physics*, 72(2):277–298, oct 1987.

[7] J. Fiedler, A. Weber, A. Bosco, K. Engel, and F. di Mare. Numerical Simulation of the Flow in the Row Labyrinth Seal of an Axial Turbine Using a Low-Mach Preconditioning Technique. In *Proceedings of TurboExpo 2016*. jun 2016.

[8] P. Sivel, C. Frey, E. Kügeler, and M. Keil. Low mach preconditioning for turbomachinery flow simulations with cavities and variable gas compositions. In *Volume 10C: Turbomachinery Design Methods and CFD Modeling for Turbomachinery; Ducts, Noise, and Component Interactions*, GT2022. June 2022.

[9] M. S. Campobasso and M. H. Baba-Ahmadi. Analysis of unsteady flows past horizontal axis wind turbine airfoils based on harmonic balance compressible navier-stokes equations with low-speed preconditioning. *Journal of Turbomachinery*, 134(6), sep 2012.

[10] J. Howison and K. Ekici. Unsteady analysis of wind turbine flows using the harmonic balance method. In *51st AIAA Aerospace Sciences Meeting including the New Horizons Forum and Aerospace Exposition*. jan 2013.

[11] R. Djeddi, J. Howison, and K. Ekici. A fully coupled turbulent low-speed preconditioner for harmonic balance applications. *Aerospace Science and Technology*, 53:22–37, jun 2016.

[12] M. Potsdam, V. Sankaran, and S. Pandya. Unsteady Low Mach Preconditioning with Application to Rotorcraft Flows. volume 2, 06 2007. ISBN 978-1-62410-129-8.

[13] E. Turkel. Preconditioning Techniques in Computational Fluid Dynamics. *Annual Review of Fluid Mechanics*, 31(1):385–416, 1999.

[14] J. M. Weiss and W. A. Smith. Preconditioning applied to variable and constant density flows. *AIAA Journal*, 33(11):2050–2057, nov 1995.

[15] D. Darmofal and K. Siu. A robust multigrid algorithm for the euler equations with local preconditioning and semi-coarsening. *Journal of Computational Physics*, 151(2):728–756, may 1999.

[16] P. L. Roe. Approximate Riemann solvers, parameter vectors, and difference schemes. *Journal of Computational Physics*, 43(2):357–372, oct 1981.

[17] J. Hope-Collins and L. di Mare. Artificial diffusion for convective and acoustic low Mach number flows I: Analysis of the modified equations, and application to Roe-type schemes. *Journal of Computational Physics*, 475:111858, feb 2023.

[18] A. Godfrey, R. Walters, and B. van Leer. Preconditioning for the Navier-Stokes equations with finite-rate chemistry. In *31st Aerospace Sciences Meeting*. jan 1993.

[19] C. Viozat. Implicit Upwind Schemes for Low Mach Number Compressible Flows. Technical Report RR-3084, INRIA, January 1997.

[20] K. Becker, K. Heitkamp, and E. Kügeler. Recent Progress In A Hybrid-Grid CFD Solver For Turbomachinery Flows. In J. C. F. Pereira, A. Sequeira, and J. M. C. Pereira, editors, *V European Conference on Computational Fluid Dynamics ECCOMAS CFD 2010*, Juni 2010.

[21] D. Canuto and K. Taira. Two-dimensional compressible viscous flow around a circular cylinder. *Journal of Fluid Mechanics*, 785:349–371, November 2015.

[22] U. Fey, M. König, and H. Eckelmann. A new strouhal-reynolds-number relationship for the circular cylinder in the range 47<re<2e5. *Physics of Fluids*, 10(7):1547–1549, jul 1998.

[23] K. Hejranfar and R. Kamali-Moghadam. Preconditioned characteristic boundary conditions for solution of the preconditioned Euler equations at low Mach number flows. *Journal of Computational Physics*, 231(12):4384–4402, jun 2012.

[24] C. Norberg. Flow around a circuler cylinder: Aspects of fluctuating lift. *Journal of Fluids and Structures*, 15(3-4):459–469, apr 2001.

[25] B. van Leer. Towards the ultimate conservative difference scheme. V. A second-order sequel to Godunovś method. *Journal of Computational Physics*, 32(1):101–136, July 1979.

[26] G. van Albada, B. van Leer, and W. Roberts. A comparative study of computational methods in cosmic gas dynamics. *Astronomy and Astrophysics*, 108:76–84, 04 1982.

[27] C. H. K. Williamson. Defining a universal and continuous strouhal–reynolds number relationship for the laminar vortex shedding of a circular cylinder. *Physics of Fluids*, 31(10): 2742, 1988.